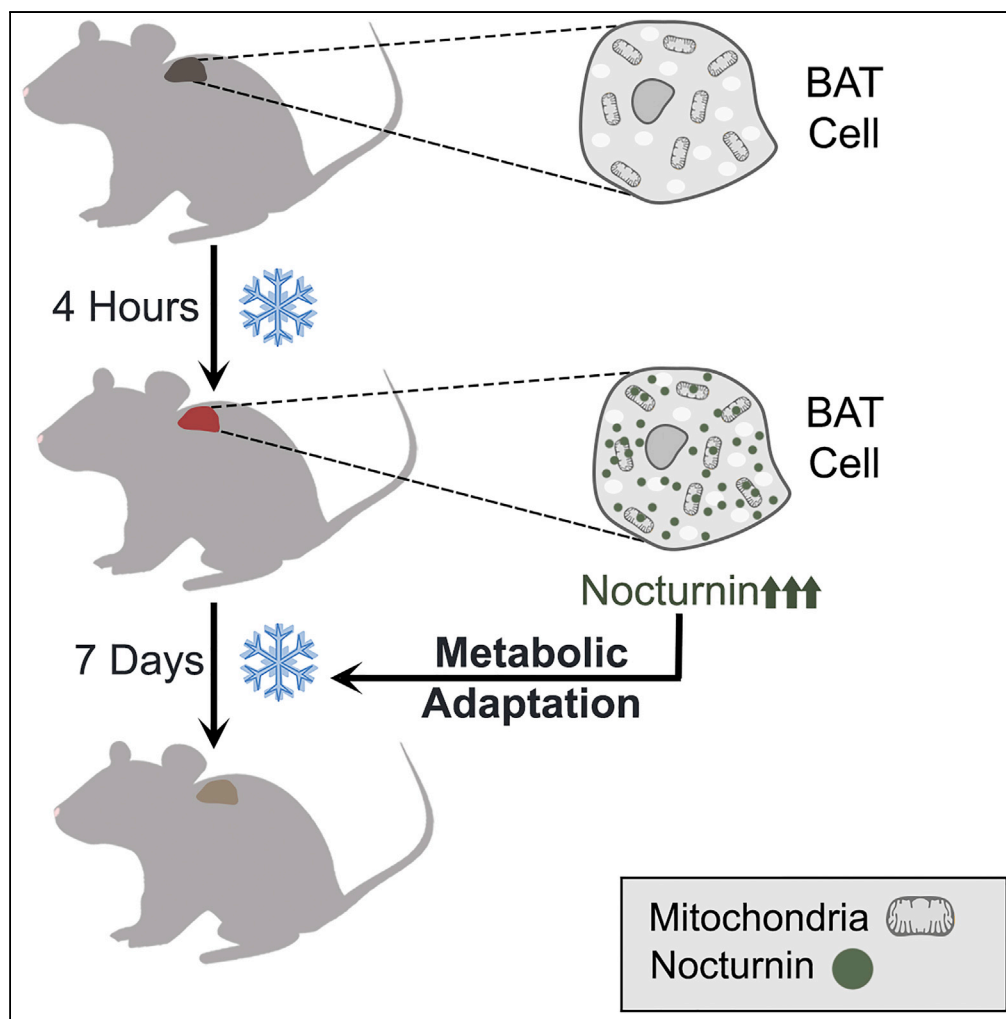**Article**

The Circadian Protein Nocturnin Regulates Metabolic Adaptation in Brown Adipose Tissue

Yasemin Onder,
Isara Laothamatas,
Stefano Berto, ...,
Genevieve
Konopka,
Prashant Mishra,
Carla B. Green

prashant.mishra@
utsouthwestern.edu (P.M.)
carla.green@utsouthwestern.
edu (C.B.G.)

HIGHLIGHTS

Nocturnin localizes to both the cytosol and the mitochondria

Nocturnin is robustly induced in response to cold exposure in brown fat

Regulation of mitochondrial metabolic genes is altered in *Nocturnin*$^{-/-}$ brown fat

Nocturnin regulates long-term metabolic adaptation to cold exposure in brown fat

DATA AND CODE
AVAILABILITY
GSE133050

Article

The Circadian Protein Nocturnin Regulates Metabolic Adaptation in Brown Adipose Tissue

Yasemin Onder,[1] Isara Laothamatas,[1] Stefano Berto,[1] Katharina Sewart,[1] Gokhul Kilaru,[1] Bogdan Bordieanu,[2] Jeremy J. Stubblefield,[3] Genevieve Konopka,[1] Prashant Mishra,[2,4,5,*] and Carla B. Green[1,6,*]

SUMMARY

Fine-tuning of transcriptional responses can be critical for long-term outcomes in response to an environmental challenge. The circadian protein Nocturnin belongs to a family of proteins that include exonucleases, endonucleases, and phosphatases and is most closely related to the CCR4 family of deadenylases that regulate the cellular transcriptome via control of poly(A) tail length of RNA transcripts. In this study, we investigate the role of Nocturnin in regulating the transcriptional response and downstream metabolic adaptations during cold exposure in brown adipose tissue. We find that Nocturnin exhibits dual localization within the cytosol and mitochondria, and loss of Nocturnin causes changes in expression of networks of mRNAs involved in mitochondrial function. Furthermore, Nocturnin$^{-/-}$ animals display significantly elevated levels of tricarboxylic acid cycle intermediates, indicating that they have distinct metabolic adaptations during a prolonged cold exposure. We conclude that cold-induced stimulation of Nocturnin levels can regulate long-term metabolic adaptations to environmental challenges.

INTRODUCTION

Circadian rhythms allow organisms to adapt to daily alterations in the environment, including changes in energy demand, and are critical for metabolic homeostasis. Indeed, disruptions in circadian rhythms are often correlated with metabolic disorders (Brum et al., 2015; Karlsson et al., 2001; Lamia et al., 2008; Marcheva et al., 2010; Mukherji et al., 2015; Oishi et al., 2006; Rorbach and Minczuk, 2012; Rudic et al., 2004; Turek et al., 2005). Nocturnin (*Noct, Ccrn4l*) is widely conserved among eukaryotes and is expressed ubiquitously in many mammalian tissues (Baggs and Green, 2003; Wang et al., 2001). As a highly rhythmic output gene of the core circadian clock machinery (Oishi et al., 2003), *Nocturnin* mRNA levels peak at early night in mice. However, it has also been identified as an immediate-early gene, and it is acutely induced in response to numerous stimuli, including serum deprivation, lipopolysaccharide, and peroxisome proliferator-activated receptor γ (PPARγ) agonist rosiglitazone (Garbarino-Pico et al., 2007; Kawai et al., 2010b; Niu et al., 2011). *Nocturnin* can also be induced by nutrient and metabolic cues, such as high-fat diet and olive oil gavage (Douris et al., 2011; Green et al., 2007; Stubblefield et al., 2018). Analysis of *Nocturnin*$^{-/-}$ animals has provided evidence for a role in numerous physiologic processes, including lipid metabolism (Green et al., 2007; Stubblefield et al., 2018), adipogenesis (Kawai et al., 2010b), osteogenesis (Kawai et al., 2010a), and immune function (Niu et al., 2011).

Nocturnin belongs to a family of proteins that include exonucleases, endonucleases, and phosphatases and is most closely related to the CCR4 family of deadenylases, which remove poly(A) tails from mRNAs (Baggs and Green, 2003; Godwin et al., 2013). This potential function and its capacity to respond to environmental cues make Nocturnin a candidate for fine-tuning transcriptional responses to metabolic challenges. By shortening the length of mRNA poly(A) tails, Nocturnin is predicted to destabilize its target mRNAs. RNA sequencing (RNA-seq) analysis of *Nocturnin*$^{-/-}$ mouse liver revealed increased amplitudes in the daily rhythms of many enzymes regulating triglyceride and cholesterol synthesis, as well as an increased amplitude in response to a fasting-refeeding challenge (Stubblefield et al., 2018). This has led to the model that modulation of Nocturnin levels allows for post-transcriptional regulation of metabolic flux. In this study, we investigate the role of Nocturnin in mediating metabolic adaptation in brown adipose tissue (BAT). We find that Nocturnin exhibits dual localization within cells, with a portion of the protein targeted to the mitochondrion. *Nocturnin* is acutely induced in BAT in response to cold exposure, and a

[1]Department of Neuroscience, University of Texas Southwestern Medical Center, Dallas, TX 75390, USA

[2]Children's Medical Center Research Institute, University of Texas Southwestern Medical Center, Dallas, TX 75390, USA

[3]Department of Cell Systems & Anatomy, UT Health San Antonio, San Antonio, TX 78229, USA

[4]Department of Pediatrics, University of Texas Southwestern Medical Center, Dallas, TX 75390, USA

[5]The Green Center for Systems Biology, University of Texas Southwestern Medical Center, Dallas, TX 75390, USA

[6]Lead Contact

*Correspondence:
prashant.mishra@utsouthwestern.edu (P.M.),
carla.green@utsouthwestern.edu (C.B.G.)

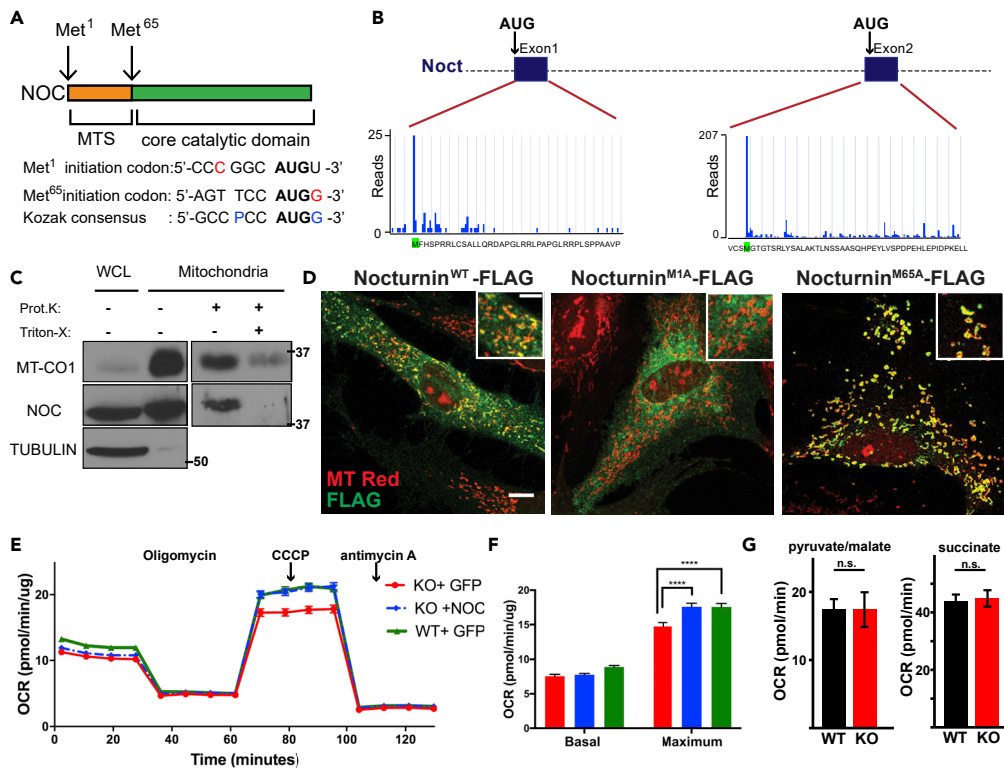https://doi.org/10.1016/j.isci.2019.07.016

Figure 1. Nocturnin Localizes to Both the Mitochondria and Cytosol via the Use of Alternative Translation Initiation Sites

(A) Nocturnin contains two potential initiation codons (Met[1] and Met[65]), separated by a mitochondrial targeting sequence. Nucleotides in red show the critical components of the Kozak sequence: a purine (A or G) at position −3 and a G following the AUG start codon.

(B) Quantitative translation initiation sequencing (QTI-seq) analysis of human Nocturnin; graphs and data reproduced from GWIPS-viz database (Michel et al., 2014).

(C) Proteinase K (Prot.K) protection assay of the mitochondrial fraction from HEK293 cells. Mitochondrial fractions were treated with Proteinase K (100 μg/mL) or Triton X-100 (1%), and samples were blotted for MT-CO1 (mitochondrial) and TUBULIN (cytoplasmic) as controls. WCL, whole-cell lysate. Molecular weight markers are indicated in kilodaltons.

(D) Nocturnin^{−/−} MEFs expressing exogenous versions of Nocturnin were stained with MitoTracker (red; mitochondria), FLAG antibody (green; NOCTURNIN). Scale bar, 21μM.

(E) Oxygen consumption rates (normalized to protein concentration) in cells of the indicated genotype. Oligomycin, CCCP (carbonyl cyanide m-chlorophenylhydrazone), and antimycin A were injected at the indicated times.

(F) Bar graph showing averages for basal and maximum respiration. A representative experiment from three independent experiments is shown.

(G) State 4 respiration from permeabilized cells of the indicated genotype in response to complex I (pyruvate/malate) or complex II (succinate) substrates.

N = 16–23 per group, ****p < 0.0001, p values are calculated by two-way ANOVA followed by Tukey's post-hoc test. Data are represented as mean ± SEM; n.s., not significant. See also Figure S1.

combination of transcriptomic and metabolic analyses indicate that it regulates long-term metabolic adaptation to cold exposure.

RESULTS

Nocturnin Localizes to Both the Mitochondria and Cytosol

Analysis of *Nocturnin*'s mRNA sequence reveals two potential in-frame translation initiation codons near the 5' end in exons 1 and 2, separated by 64 amino acids (Figure 1A). Both start codons are surrounded by sequences that diverge from the canonical Kozak sequence. From publicly available quantitative translation initiating ribosome profiling data (Crappe et al., 2015; Fijalkowska et al., 2017; Gao et al., 2015; Gawron et al., 2016; Ji et al., 2015; Raj et al., 2016; Zhang et al., 2017), we found that global aggregate from human cell lines indicated peaks of ribosome occupancy at both methionines, referred to as Met[1] and

Met[65] (numbering based on *Mus musculus* sequence) (Figure 1B). In addition, elongating ribosomes are readily observed in exon 1, before Met[65] (Figure S1A). Analysis of Nocturnin's amino acid sequence (starting at Met[1]) predicts a putative mitochondrial targeting sequence within the first 65 amino acids, as determined by multiple prediction programs (Figures 1A and S1B). Thus, we hypothesized that the choice of start codon determines Nocturnin's subcellular localization. We carried out biochemical fractionation of HEK293 cells to separate the mitochondrial and cytosolic fractions, followed by a Proteinase K protection assay on the mitochondrial fraction (Figure 1C). A portion of Nocturnin was significantly enriched in the mitochondrial fraction and protected from degradation upon Proteinase K treatment, confirming that Nocturnin localizes within the mitochondrial membrane.

We transduced *Nocturnin*^{−/−} mouse embryonic fibroblasts (MEFs) with lentivirus expressing FLAG-tagged Nocturnin[wt], as well as FLAG-tagged Nocturnin[M1A] or Nocturnin[M65A], to force translation initiation at the second or first start codon, respectively (Figure 1D). Nocturnin[M1A] localized to the cytoplasm exclusively, whereas Nocturnin[M65A] exhibited predominant mitochondrial localization (as detected by overlap with MitoTracker Red). Cells expressing wild-type Nocturnin exhibited both cytoplasmic and mitochondrial localization. Thus the choice of initiation codon is sufficient to determine Nocturnin's subcellular localization.

Nocturnin's localization to the mitochondrion suggests a potential role in mitochondrial function, and mitochondrial mRNAs are exclusively utilized for the production of components of the electron transport chain. Oxygen consumption measurements in *Nocturnin*^{−/−} MEFs revealed no significant differences in basal respiration, but a mild reduction in uncoupled respiration (induced by CCCP [carbonyl cyanide *m*-chlorophenylhydrazone]) (Figures 1E and 1F). Stable re-expression of Nocturnin (Figure S1C) (in *Nocturnin*^{−/−} MEFs) was sufficient to rescue the defect in uncoupled respiration (Figures 1E and 1F). We therefore used permeabilized cells to assess organellar function in wild-type and *Nocturnin*^{−/−} MEFs. Analysis of state 4 (uncoupled) mitochondrial respiration (Figure 1G) revealed no defects in complex I (pyruvate/malate) or complex II (succinate) stimulated respiration, indicating that the mild respiratory defect observed in intact cells is due to metabolic alterations, as opposed to inherent reductions in mitochondrial function.

Nocturnin mRNA Is Acutely Induced in Brown Adipose Tissue Following Cold Exposure

The above results suggest that Nocturnin does not play a major role in regulating mitochondrial function in cultured MEFs but may be specifically important to metabolic control of the uncoupled state. *In vivo*, BAT is well known to use uncoupled mitochondrial respiration to generate heat in response to cold exposure via the rapid induction of mitochondrial uncoupling proteins (e.g., UCP-1). In this situation, nutrients (e.g., glucose, fatty acid) are rapidly oxidized within the tricarboxylic acid (TCA) cycle, providing substrates for the electron transport chain. Like HEK293 cells, biochemical fractionation of BAT indicated that Nocturnin is present in both cytoplasmic and mitochondrial compartments (Figure 2A). Furthermore, an acute cold-exposure protocol in mice (6°C for 4 h) revealed that *Nocturnin* transcripts are strongly induced in BAT (Figure 2B). We therefore examined the role of Nocturnin during cold exposure.

Nocturnin expression is robustly circadian with peak mRNA and protein levels at the onset of night (ZT12) in murine liver (Garbarino-Pico et al., 2007; Sinturel et al., 2017; Stubblefield et al., 2018; Wang et al., 2001; Zhang et al., 2014). In brown fat, Nocturnin mRNA is also circadian, with peak levels at ZT12 (Zhang et al., 2014). We therefore examined thermogenic responses in mice following cold exposure at two opposite phases of the circadian cycle. WT and *Nocturnin*^{−/−} mice were put in cold chambers at 1 h after light onset (ZT1) or 1 h after dark onset (ZT13), and temperatures were measured every 4 h for the following 12 h. We observed a mild deficit in thermogenic recovery in the *Nocturnin*^{−/−} mice in both conditions (Figure 2C). Thus, Nocturnin is not strictly required for cold-temperature adaptation, although adaptation mechanisms appear less robust in *Nocturnin*^{−/−} animals. Consistent with this, induction of known cold-responsive genes was largely intact in *Nocturnin*^{−/−} mice, although some genes (e.g., *Pparγ*) exhibited reduced responsiveness (Figure 2D).

Nocturnin's putative function as a deadenylase suggests a role in post-transcriptional regulation of mRNA stability via control of poly(A) tail length (Baggs and Green, 2003). Twelve of the 13 mRNAs (*ND6* is the exception) encoded by the mitochondrial genome are polyadenylated with poly(A) tails shorter than those found on nuclear-encoded mRNAs in the cytoplasm, although the exact role of these tails is still being debated (Rorbach and Minczuk, 2012). We therefore measured levels of mitochondrial RNA (mtRNA) species in the two genotypes at room temperature and following cold exposure. There were no apparent
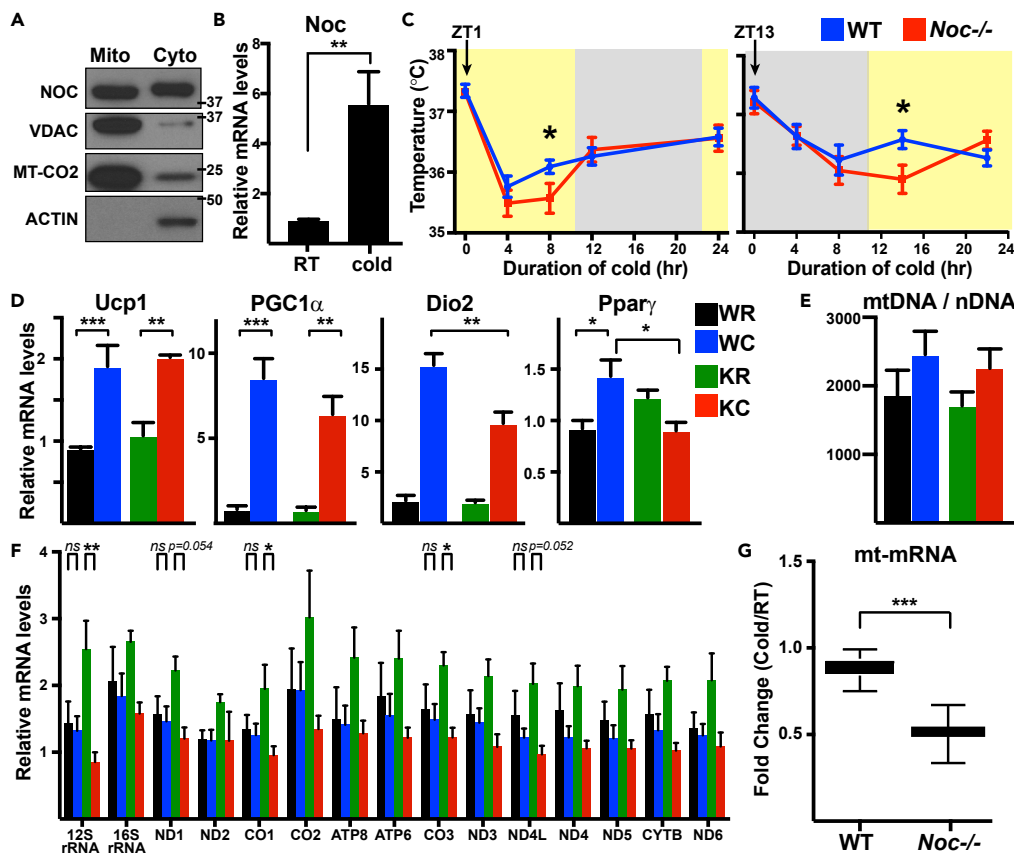
Figure 2. *Nocturnin* Is Induced in BAT in Response to Acute Cold Exposure

(A) Biochemical fractionation of mitochondrial and cytoplasmic compartments in wild-type BAT, blotted for NOC, VDAC (mitochondrial outer membrane), MT-CO2 (mitochondrial matrix), and ACTIN (cytoplasm) proteins. Molecular weight markers are indicated in kilodaltons.

(B) qRT-PCR analysis of BAT samples from wild-type and *Nocturnin*$^{-/-}$ littermates kept at room temperature (RT) or exposed to cold (6°C) for 4 h.

(C) Core body temperature of mice during prolonged cold exposure at 6°C; animals placed at cold at ZT1 (left) or ZT13 (right) (N = 8–10/genotype, yellow and gray shading indicating day and night, respectively).

(D) Transcript levels of *Ucp1*, *Ppar*γ, *PGC1*α, and *Dio2* genes normalized to *B2M* in BAT tissue of the indicated genotype and condition (N = 3–6). WR, wild-type room temperature; WC, wild-type cold; KR, *Nocturnin*$^{-/-}$ room temperature; KC, *Nocturnin*$^{-/-}$ cold.

(E) mtDNA copy numbers in BAT of mice kept at RT or cold (6°C, 4h) (N = 4–5).

(F) qRT-PCR analysis of mitochondrial-encoded genes in BAT. Transcript levels were normalized to mtDNA copy number. (N = 3–5).

(G) Average fold changes for mtDNA genes in response to a 4-h cold exposure in the indicated genotypes.

*p < 0.05, **p < 0.01, ***p < 0.001, ****p < 0.0001 as analyzed by two-way analysis of variance (ANOVA) with a Tukey's post-hoc test (A, D, and F) or two-tailed Student's t test (C and G). Data are represented as mean ± SEM; ns, not significant.

defects in mitochondrial genome content in *Nocturnin*$^{-/-}$ BAT (Figure 2E), suggesting that mitochondrial biogenesis is unchanged. However, whereas levels of mtRNA species did not change significantly in response to cold exposure in the WT mice, the mtRNAs in the *Nocturnin*$^{-/-}$ BAT were modestly affected by temperature, with globally elevated levels in room temperature-housed mice and global decreases following cold exposure (Figures 2F and 2G).

Regulation of Mitochondrial Metabolic Genes Is Altered in *Nocturnin*$^{-/-}$ BAT

The acute induction of *Nocturnin* in response to cold (Figure 2B) suggests that it may regulate the overall transcriptional response to cold exposure. We performed mRNA-seq analysis on BAT isolated from wild-type and *Nocturnin*$^{-/-}$ littermates at room temperature or after a 4-h cold challenge. Differential
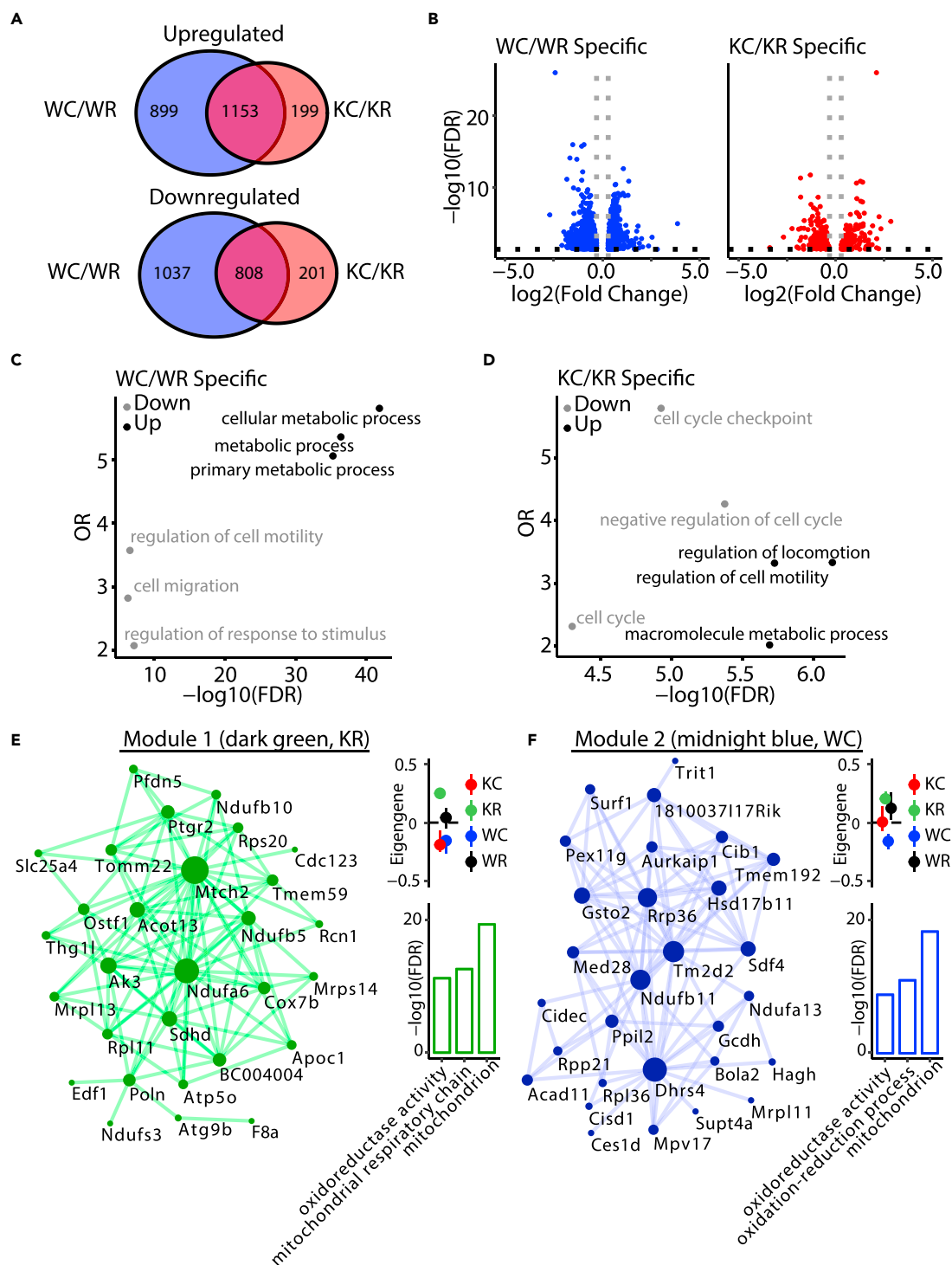
Figure 3. Altered Expression of Mitochondrial Metabolic Genes in *Nocturnin*^{−/−} BAT Following Cold Exposure

(A) Venn diagrams of common and unique genes that are differentially expressed following 4-h cold exposure in wild-type (WC/WR) and *Nocturnin*^{−/−} (KC/KR) BAT. Top: Venn diagram of upregulated genes. Bottom: Venn diagram, downregulated genes. Blue, WT; red, *Nocturnin*^{−/−}. WR, wild-type room temperature; WC, wild-type cold; KR, *Nocturnin*^{−/−} room temperature; KC, *Nocturnin*^{−/−} cold.

(B) Volcano plot for uniquely changing genes in WT and *Nocturnin*^{−/−} BAT following 4-h cold exposure. y axis represents $-\log_{10}$(FDR). x axis represent $\log_2$(fold change) from differential expression analysis statistics.

Figure 3. *Continued*

(C and D) Functional enrichment analyses of uniquely differentially expressed genes in (C) WT (# of genes = 1,935) and (D) *Nocturnin*$^{-/-}$ (# of genes = 399). Downregulated pathways are shown in gray; upregulated pathways are shown in black. y axis represents odds ratios (OR). x axis represents –$\log_{10}$(FDR). The top three most significant categories are shown.

(E and F) Visualization of the top 100 connections ranked by weighted topological overlap values for module 1 (dark green, KR correlated) and module 2 (midnight blue, WC correlated). Node size corresponds to the number of edges (*degree*). Side dot plots with standard errors demonstrate the association of the modules detected with genotype and temperature. Standard errors are calculated based on the eigengene across samples. Dots represent the mean eigengene for that module. Side bar plots show the top three gene ontology groups of the module based on –$\log_{10}$(FDR). FDR, false discovery rate.

See also Tables S1 and S2.

expression analysis between the two temperatures revealed some changes in the transcriptional response to cold between wild-type and *Nocturnin*$^{-/-}$ animals (Figures 3A and 3B and Table S1). Many of the mRNAs that showed altered levels in response to temperature were not different between genotypes, and among those genes that were uniquely regulated in either wild-type or *Nocturnin*$^{-/-}$ animals, similar gene ontology pathways were represented (Figures 3C and 3D, Table S1). Thus the overall transcriptional response to acute cold exposure is largely conserved in *Nocturnin*$^{-/-}$ animals, with only subtle changes.

To determine whether there might be gene expression changes driven by the intersection of genotype and temperature at the network level, we performed weighted gene co-expression network analysis (Fontenot et al., 2017; Langfelder and Horvath, 2008) (Table S2). We identified two modules with gene expression patterns driven by samples with a specific combination of genotype and temperature. Module 1 (dark green, Figure 3E) represents genes most highly correlated in the *Nocturnin*$^{-/-}$ BAT room-temperature samples (see eigengene inset). Module 2 (midnight blue, Figure 3F) represented genes most highly correlated in wild-type BAT cold samples. Interestingly, whereas the dark green and midnight blue modules contain completely independent genes, ontology analysis indicates that both modules are highly enriched in genes linked to mitochondrial function (Figures 3E and 3F, Table S2).

Metabolomics Analysis Reveals Altered Long-Term Metabolic Adaptation in *Nocturnin*$^{-/-}$ BAT

The network analysis above suggests a metabolic role for Nocturnin induction during cold exposure. We therefore performed targeted metabolomics measurements in BAT from wild-type and *Nocturnin*$^{-/-}$ mice in response to a 4-h cold exposure (Figure 4A, Table S3). Unsupervised hierarchical clustering and principal-component analysis (PCA) reliably separated room-temperature and cold-exposure samples but could not distinguish wild-type and *Nocturnin*$^{-/-}$ genotypes (Figures 4A and 4B). These results indicate that the overall metabolic response to acute cold exposure is largely maintained in *Nocturnin*$^{-/-}$ BAT.

As Nocturnin's putative function invokes regulation of mRNA stability, we hypothesized that its induction during cold exposure may play a role during longer-term adaptations. To examine this possibility, we assessed animals subject to a prolonged cold exposure (7 days). *Nocturnin*$^{-/-}$ animals did not display any defects in core body temperature or body weight during this challenge (Figures S2A and S2B). Despite this, steady-state metabolomics revealed striking differences between wild-type and *Nocturnin*$^{-/-}$ BAT (Figures 4C and 4D, Table S3): Unsupervised hierarchical clustering and PCA revealed that *Nocturnin*$^{-/-}$ BAT clusters distinctly from other conditions after a 7-day cold exposure. Interestingly, 7-day cold wild-type BAT appears to occupy an intermediate position between room-temperature groups and 7-day cold *Nocturnin*$^{-/-}$ BAT (Figures 4C and 4D), indicating that long-term metabolic adaptation in *Nocturnin*$^{-/-}$ BAT is distinct and more profound than in wild-type BAT. To assess the relevant metabolic pathways mediating separation of 7-day cold *Nocturnin*$^{-/-}$ BAT, we focused on principal component 1 (PC1) in the PCA, which reliably separates these groups. Of the top 10 metabolites contributing to PC1, seven reflect intermediates in the mitochondrial TCA cycle (Figure 4E). This pattern was specific to the 7-day analysis (Figures S3A and S3B). We therefore compared patterns of TCA metabolite abundances in 4-h and 7-day cold-exposure cohorts. BAT is known to readily use succinate as a key mitochondrial fuel source during acute cold exposure (Mills et al., 2018), and *Nocturnin*$^{-/-}$ animals maintained this metabolic signature (Figure 4F), consistent with their overall ability to maintain thermogenesis. However, succinate levels in wild-type BAT were relatively blunted after 7 days, whereas *Nocturnin*$^{-/-}$ BAT displayed continued striking increases in succinate levels, accompanied by similar increases in other TCA cycle metabolites (Figure 4G). Consistent with this model, *Slc25a10*, the mitochondrial dicarboxylate carrier responsible for succinate entry into the mitochondria, is specifically downregulated in wild-type, but not
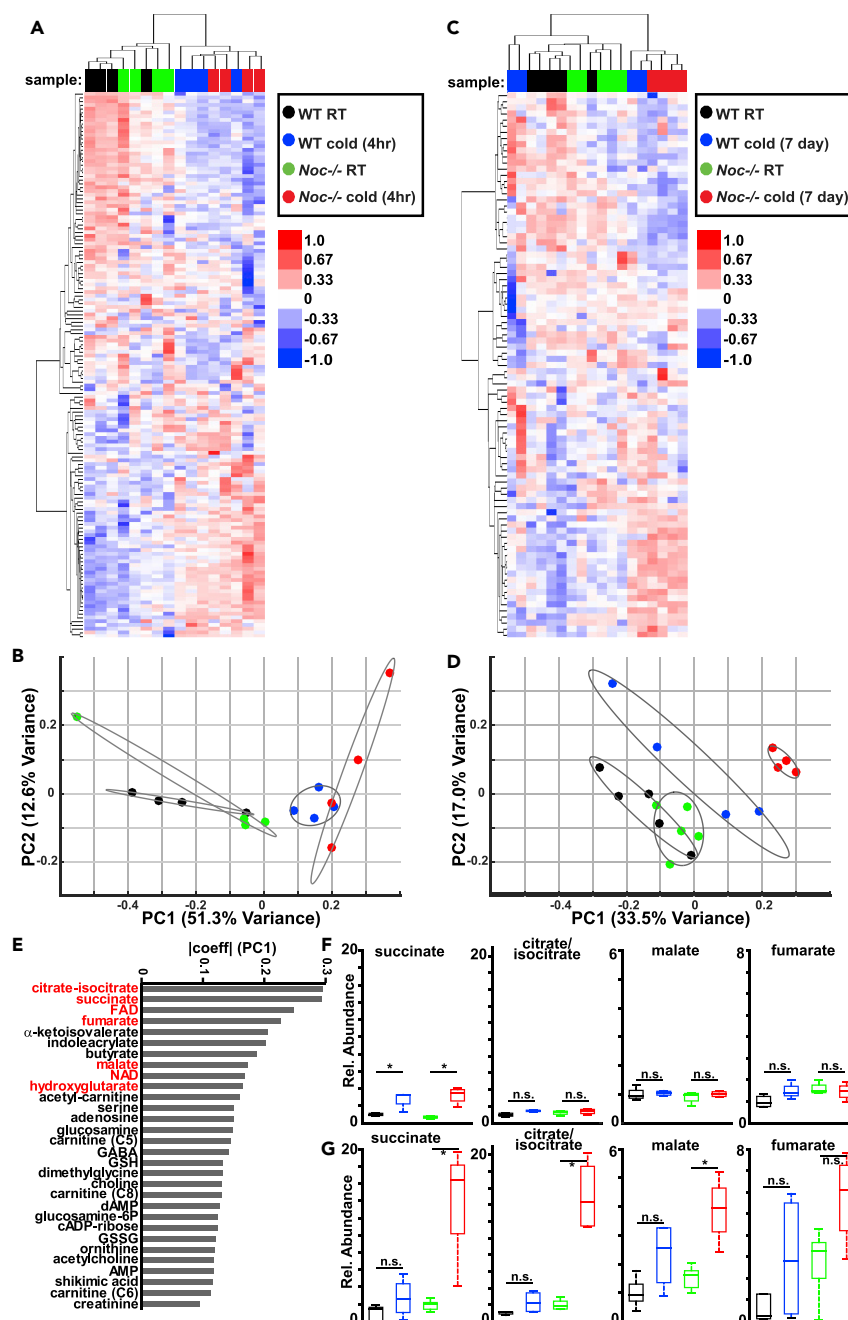
Figure 4. Tricarboxylic Acid Cycle Intermediates Are Altered in *Nocturnin*⁻/⁻ BAT in Response to Prolonged Cold Exposure

(A) Heatmap representing hierarchical clustering of normalized metabolite abundances from the indicated genotypes, subject to room temperature (RT) or a 4-h cold exposure. Color bar reflects log-transformed abundance levels. Sample identity is indicated at the top of each column.

(B) Principal-component analysis of wild-type and *Nocturnin*⁻/⁻ BAT subject to RT or a 4-h cold exposure. Ovals represent 95% confidence intervals. Contribution of each principal component to total variance is indicated. Same color scheme as (A).

(C) Heatmap representing hierarchical clustering of normalized metabolite abundances from the indicated genotypes, subject to RT or a 7-day cold exposure. Color bar reflects log-transformed abundances. Sample identity is indicated at the top of each column.

Figure 4. Continued

(D) Principal-component analysis of wild-type and *Nocturnin*⁻/⁻ BAT subject to RT or a 7-day cold exposure. Same color scheme as (C). Ovals represent 95% confidence intervals. Contribution of each principal component to total variance is indicated.

(E) Contribution of the top 30 metabolites contributing to principal component 1 (PC1) for the principal component analysis of 7-day metabolomics shown in (D). Mitochondrial TCA-related metabolites are shown in red. Absolute magnitude of coefficients for each metabolite for PC1 (7-day) are plotted.

(F) Normalized abundances for select TCA metabolites in wild-type and *Nocturnin*⁻/⁻ BAT subject to RT or a 4-h cold exposure. Boxplots display the median, 25th and 75th percentiles, and the range for metabolite levels. Same color scheme as (A). N = 4/genotype. *p < 0.05, as analyzed by analysis of variance (ANOVA) with a Tukey's post-hoc test; n.s., not significant.

(G) Same as (F), but for BAT subject to RT or a 7-day cold exposure. Same color scheme as (B). N = 4–5/genotype. *p < 0.05, as analyzed by analysis of variance (ANOVA) with a Tukey's post-hoc test.

See also Figures S2 and S3 and Table S3.

Nocturnin⁻/⁻, animals after 4-h cold exposure (Figure S2C). Thus, we propose that whereas BAT metabolism is profoundly altered in response to an acute cold exposure, the induction of *Nocturnin* serves to suppress the acute metabolic response in the case of long-term cold exposure, thereby mediating long-term adaptation.

DISCUSSION

Our results indicate that the induction of *Nocturnin* is non-essential during cold exposure in mice, but plays a role in regulating long-term metabolic adaptation of BAT. Mechanistically, the precise function and targets of Nocturnin are unknown, although it has been implicated in de-stabilizing mRNAs (via control of poly(A) tail lengths) as well as circadian control of metabolic enzymes. Tuning of transcriptional responses via regulation of mRNA stability may be important for the long-term outcome to an environmental challenge, and this role for Nocturnin may underlie its role in long-term metabolic adaptation. Alternatively, Nocturnin may have a more direct function in controlling metabolic activity. In addition, dual localization within the cytosol and mitochondria allows Nocturnin to potentially coordinate metabolism in different compartments. Studies examining BAT with exclusively localized mitochondrial versus cytosolic Nocturnin will be need to validate this model. However, the relatively subtle changes in gene expression observed in *Nocturnin*⁻/⁻ animals suggest that loss of this gene is having an indirect effect on mitochondrial metabolism rather than targeting a few specific transcripts.

In the setting of cold exposure, BAT must rapidly oxidize nutrients within the mitochondrion to generate heat and maintain body temperature. Recent reports indicate that muscle-derived succinate serves as an important substrate during the acute cold response and that exogenous administration of succinate is sufficient to promote thermogenesis and weight loss (Mills et al., 2018). Acute utilization of succinate appears intact in *Nocturnin*⁻/⁻ animals, whereas wild-type animals appear to downregulate succinate oxidation in the long term, perhaps shifting to alternative carbon sources. We hypothesize then that Nocturnin induction serves to limit the amplitude of the initial cold response. In this model, Nocturnin's role in multiple compartments allows for fine-tuning of metabolic adaptations during a prolonged environmental challenge. Despite the striking differences observed in metabolite levels, we observed no overt phenotypes related to body weight or core body temperature in *Nocturnin*⁻/⁻ animals subject to prolonged cold. Importantly, steady-state metabolite levels are not directly indicative of pathway flux, and future experiments using *in vivo* isotope tracing techniques will be required to validate specific mechanisms of metabolic adaptation.

Limitations of the Study

It is important to mention that energy balance and temperature are tightly regulated via hypothalamus and systemic cues, and the lack of obvious phenotypes in *Nocturnin*⁻/⁻ animals could be due to compensatory mechanisms such as browning of white adipose tissue or muscle-based thermogenesis. Whether the phenotypes we observe are due to Nocturnin function in the mitochondria, the cytoplasm, or both cannot be determined by the experiments proposed here and will require the generation of mice expressing specific isoforms. In addition, a significant limitation of our study is that our comparisons were made between subjects at 6°C and room temperature, as opposed to thermoneutral animals (∼30°C). In addition, rectal temperature measurements predominantly reflect whole-body temperature and are subject to handling-induced stress, whereas telemetry measurements of BAT temperature will provide a more robust and direct

measurement of BAT function. In the future, a detailed phenotypic analysis of BAT in *Nocturnin*$^{-/-}$ mice will be important to evaluate the functional importance of Nocturnin during long-term stressors.

METHODS

All methods can be found in the accompanying Transparent Methods supplemental file.

DATA AND CODE AVAILABILITY

All data supporting the findings of this study are available within the article, extended data files, or available from the corresponding author upon reasonable request. The NCBI Gene Expression Omnibus (GEO) accession number for the RNA-seq data reported in this study is GSE133050 (token: ymregeultsvtih).

SUPPLEMENTAL INFORMATION

Supplemental Information can be found online at https://doi.org/10.1016/j.isci.2019.07.016.

AUTHOR CONTRIBUTIONS

Y.O. performed the experimental design, data collection and analysis, as well as manuscript preparation. I.L. performed the Proteinase K treatment experiment. K.S. prepared the mRNA-seq libraries and helped with mouse husbandry and genotyping. G.K. performed the mapping analysis of the mRNA-seq data. S.B. and G.K. performed bioinformatics analysis of the mRNA-seq data including the WGCNA analysis. B.B. performed the metabolomics measurements and analysis. J.J.S. and I.L. helped with tissue collections. P.M. and C.B.G. provided supervision on experimental design, data interpretation, and manuscript preparation.

DECLARATION OF INTERESTS

The authors declare no competing interests.

REFERENCES

Baggs, J.E., and Green, C.B. (2003). Nocturnin, a deadenylase in Xenopus laevis retina: a mechanism for posttranscriptional control of circadian-related mRNA. Curr. Biol. *13*, 189–198.

Brum, M.C., Filho, F.F., Schnorr, C.C., Bottega, G.B., and Rodrigues, T.C. (2015). Shift work and its association with metabolic disorders. Diabetol. Metab. Syndr. *7*, 45.

Crappe, J., Ndah, E., Koch, A., Steyaert, S., Gawron, D., De Keulenaer, S., De Meester, E., De Meyer, T., Van Criekinge, W., Van Damme, P., et al. (2015). PROTEOFORMER: deep proteome coverage through ribosome profiling and MS integration. Nucleic Acids Res. *4*, e29.

Douris, N., Kojima, S., Pan, X., Lerch-Gaggl, A.F., Duong, S.Q., Hussain, M.M., and Green, C.B.

(2011). Nocturnin regulates circadian trafficking of dietary lipid in intestinal enterocytes. Curr. Biol. *21*, 1347–1355.

Fijalkowska, D., Verbruggen, S., Ndah, E., Jonckheere, V., Menschaert, G., and Van Damme, P. (2017). eIF1 modulates the recognition of suboptimal translation initiation sites and steers gene expression via uORFs. Nucleic Acids Res. *45*, 7997–8013.

Fontenot, M.R., Berto, S., Liu, Y., Werthmann, G., Douglas, C., Usui, N., Gleason, K., Tamminga, C.A., Takahashi, J.S., and Konopka, G. (2017). Novel transcriptional networks regulated by CLOCK in human neurons. Genes Dev. *31*, 2121–2135.

Gao, X., Wan, J., Liu, B., Ma, M., Shen, B., and Qian, S.B. (2015). Quantitative profiling of

initiating ribosomes in vivo. Nat. Methods *12*, 147–153.

Garbarino-Pico, E., Niu, S., Rollag, M.D., Strayer, C.A., Besharse, J.C., and Green, C.B. (2007). Immediate early response of the circadian polyA ribonuclease nocturnin to two extracellular stimuli. RNA *13*, 745–755.

Gawron, D., Ndah, E., Gevaert, K., and Van Damme, P. (2016). Positional proteomics reveals differences in N-terminal proteoform stability. Mol. Syst. Biol. *12*, 858.

Godwin, A.R., Kojima, S., Green, C.B., and Wilusz, J. (2013). Kiss your tail goodbye: the role of PARN, Nocturnin, and Angel deadenylases in mRNA biology. Biochim. Biophys. Acta *1829*, 571–579.

Green, C.B., Douris, N., Kojima, S., Strayer, C.A., Fogerty, J., Lourim, D., Keller, S.R., and Besharse, J.C. (2007). Loss of Nocturnin, a circadian deadenylase, confers resistance to hepatic steatosis and diet-induced obesity. Proc. Natl. Acad. Sci. U S A *104*, 9888–9893.

Ji, Z., Song, R., Regev, A., and Struhl, K. (2015). Many lncRNAs, 5'UTRs, and pseudogenes are translated and some are likely to express functional proteins. Elife *4*, e08890.

Karlsson, B., Knutsson, A., and Lindahl, B. (2001). Is there an association between shift work and having a metabolic syndrome? Results from a population based study of 27 485 people. Occup. Environ. Med. *58*, 747–752.

Kawai, M., Delany, A.M., Green, C.B., Adamo, M.L., and Rosen, C.J. (2010a). Nocturnin suppresses igf1 expression in bone by targeting the 3' untranslated region of igf1 mRNA. Endocrinology *151*, 4861–4870.

Kawai, M., Green, C.B., Lecka-Czernik, B., Douris, N., Gilbert, M.R., Kojima, S., Ackert-Bicknell, C., Garg, N., Horowitz, M.C., Adamo, M.L., et al. (2010b). A circadian-regulated gene, Nocturnin, promotes adipogenesis by stimulating PPAR-gamma nuclear translocation. Proc. Natl. Acad. Sci. U S A *107*, 10508–10513.

Lamia, K.A., Storch, K.F., and Weitz, C.J. (2008). Physiological significance of a peripheral tissue circadian clock. Proc. Natl. Acad. Sci. U S A *105*, 15172–15177.

Langfelder, P., and Horvath, S. (2008). WGCNA: an R package for weighted correlation network analysis. BMC Bioinformatics *9*, 559.

Marcheva, B., Ramsey, K.M., Buhr, E.D., Kobayashi, Y., Su, H., Ko, C.H., Ivanova, G., Omura, C., Mo, S., Vitaterna, M.H., et al. (2010). Disruption of the clock components CLOCK and BMAL1 leads to hypoinsulinaemia and diabetes. Nature *466*, 627–631.

Michel, A.M., Fox, G., M Kiran, A., De Bo, C., O'Connor, P.B., Heaphy, S.M., Mullan, J.P., Donohue, C.A., Higgins, D.G., and Baranov, P.V. (2014). GWIPS-viz: development of a ribo-seq genome browser. Nucleic Acids Res. *42* (Database issue), D859–D864.

Mills, E.L., Pierce, K.A., Jedrychowski, M.P., Garrity, R., Winther, S., Vidoni, S., Yoneshiro, T., Spinelli, J.B., Lu, G.Z., Kazak, L., et al. (2018). Accumulation of succinate controls activation of adipose tissue thermogenesis. Nature *560*, 102–106.

Mukherji, A., Kobiita, A., Damara, M., Misra, N., Meziane, H., Champy, M.F., and Chambon, P. (2015). Shifting eating to the circadian rest phase misaligns the peripheral clocks with the master SCN clock and leads to a metabolic syndrome. Proc. Natl. Acad. Sci. U S A *112*, E6691–E6698.

Niu, S., Shingle, D.L., Garbarino-Pico, E., Kojima, S., Gilbert, M., and Green, C.B. (2011). The circadian deadenylase Nocturnin is necessary for stabilization of the iNOS mRNA in mice. PLoS One *6*, e26954.

Oishi, K., Atsumi, G., Sugiyama, S., Kodomari, I., Kasamatsu, M., Machida, K., and Ishida, N. (2006). Disrupted fat absorption attenuates obesity induced by a high-fat diet in Clock mutant mice. FEBS Lett. *580*, 127–130.

Oishi, K., Miyazaki, K., Kadota, K., Kikuno, R., Nagase, T., Atsumi, G., Ohkura, N., Azama, T., Mesaki, M., Yukimasa, S., et al. (2003). Genome-wide expression analysis of mouse liver reveals CLOCK-regulated circadian output genes. J. Biol. Chem. *278*, 41519–41527.

Raj, A., Wang, S.H., Shim, H., Harpak, A., Li, Y.I., Engelmann, B., Stephens, M., Gilad, Y., and Pritchard, J.K. (2016). Thousands of novel translated open reading frames in humans inferred by ribosome footprint profiling. Elife *5*, e13328.

Rorbach, J., and Minczuk, M. (2012). The post-transcriptional life of mammalian mitochondrial RNA. Biochem. J. *444*, 357–373.

Rudic, R.D., McNamara, P., Curtis, A.M., Boston, R.C., Panda, S., Hogenesch, J.B., and Fitzgerald, G.A. (2004). BMAL1 and CLOCK, two essential components of the circadian clock, are involved in glucose homeostasis. PLoS Biol. *2*, e377.

Sinturel, F., Gerber, A., Mauvoisin, D., Wang, J., Gatfield, D., Stubblefield, J.J., Green, C.B., Gachon, F., and Schibler, U. (2017). Diurnal oscillations in liver mass and cell size accompany ribosome assembly cycles. Cell *169*, 651–663.e14.

Stubblefield, J.J., Gao, P., Kilaru, G., Mukadam, B., Terrien, J., and Green, C.B. (2018). Temporal control of metabolic amplitude by nocturnin. Cell Rep. *22*, 1225–1235.

Turek, F.W., Joshu, C., Kohsaka, A., Lin, E., Ivanova, G., McDearmon, E., Laposky, A., Losee-Olson, S., Easton, A., Jensen, D.R., et al. (2005). Obesity and metabolic syndrome in circadian Clock mutant mice. Science *308*, 1043–1045.

Wang, Y., Osterbur, D.L., Megaw, P.L., Tosini, G., Fukuhara, C., Green, C.B., and Besharse, J.C. (2001). Rhythmic expression of Nocturnin mRNA in multiple tissues of the mouse. BMC Dev. Biol. *1*, 9.

Zhang, P., He, D., Xu, Y., Hou, J., Pan, B.F., Wang, Y., Liu, T., Davis, C.M., Ehli, E.A., Tan, L., et al. (2017). Genome-wide identification and differential analysis of translational initiation. Nat. Commun. *8*, 1749.

Zhang, R., Lahens, N.F., Ballance, H.I., Hughes, M.E., and Hogenesch, J.B. (2014). A circadian gene expression atlas in mammals: implications for biology and medicine. Proc. Natl. Acad. Sci. U S A *111*, 16219–16224.
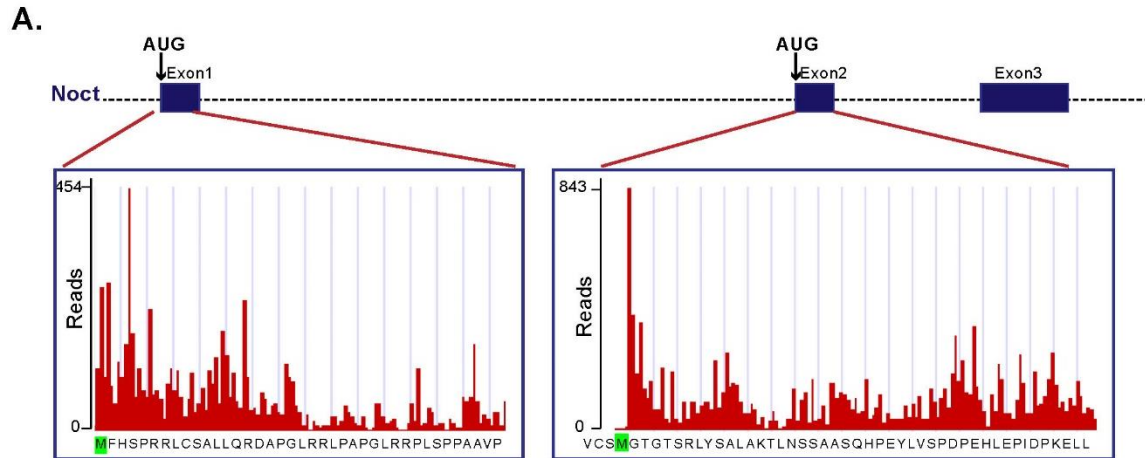
Supplemental Information

The Circadian Protein Nocturnin

Regulates Metabolic Adaptation

in Brown Adipose Tissue

Yasemin Onder, Isara Laothamatas, Stefano Berto, Katharina Sewart, Gokhul Kilaru, Bogdan Bordieanu, Jeremy J. Stubblefield, Genevieve Konopka, Prashant Mishra, and Carla B. Green

A.

B.

Ensembl Primary Identifier	Gene Symbol	Description	Organism	Mito Targeting Seq iPSORT	Mito Targeting Seq TargetP	Mito Targeting Seq MitoProt	Mito Targeting Seq MitoFates
ENSG00000151014	NOCT	nocturnin	H.sapiens	1	0.923	0.9864	0.942
ENSMUSG00000023087	Noct	Nocturnin	M. musculus	1	0.873	0.9821	0.733

C.

Figure S1, related to Figure 1.

(A) Global aggregate for elongating ribosome profiles from all studies in human cell lines, reproduced from GWIPS-viz database (Michel et al., 2014). (B) Mitochondrial targeting sequence predictions reproduced from MitoMiner 4.0 database (Smith and Robinson, 2016). (C) Confirmation of stable Nocturnin expression in the *Nocturnin*^{-/-} MEFs expressing rescue constructs as measured by western blot.

Figure S2, related to Figure 4
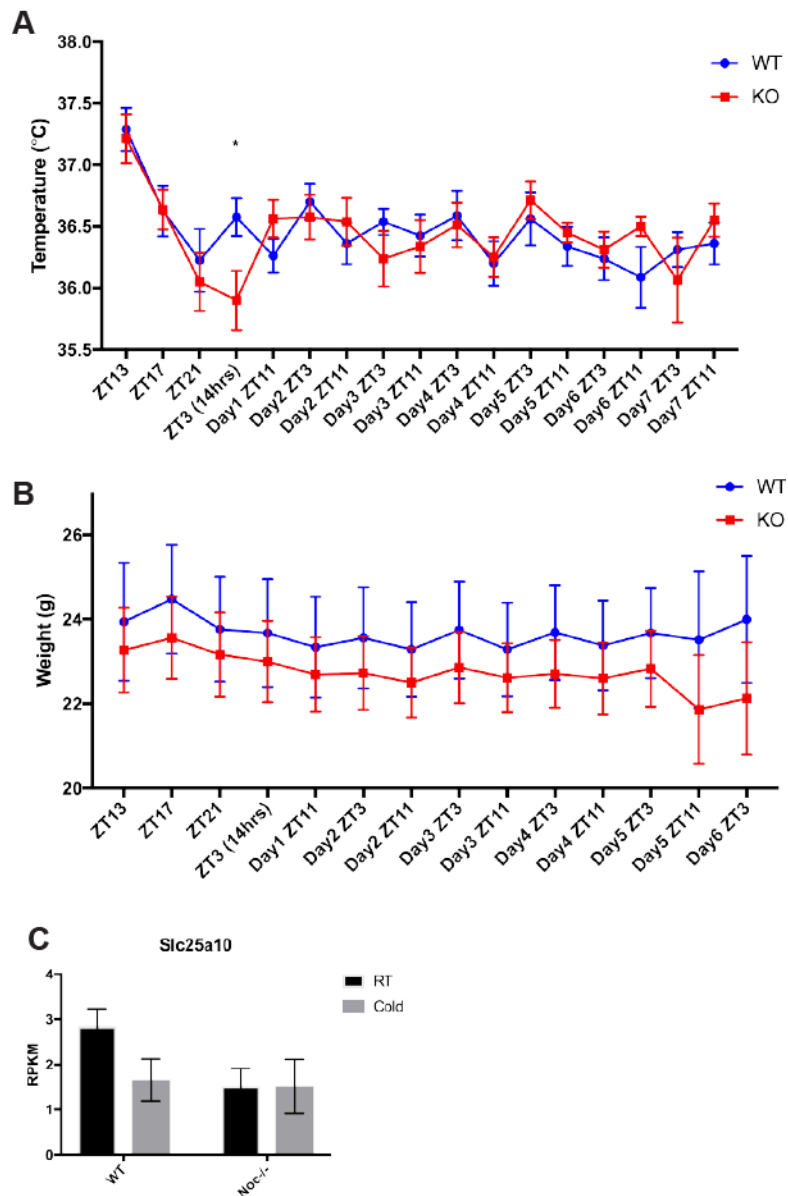
(A) Bi-daily (ZT3, ZT11) measurements of core body temperature in wild-type and *Nocturnin*^{-/-} mice kept at 6°C for 7 days. (B) Bi-daily (ZT3, ZT11) measurements of bodyweight of wild-type and *Nocturnin*^{-/-} mice kept at 6°C for 7 days. (C) RPKM values for Slc25a10 gene expression in *Nocturnin*^{-/-} and WT mice BAT kept at RT or cold conditions for 4hrs. Data represent mean +/- s.e.m.
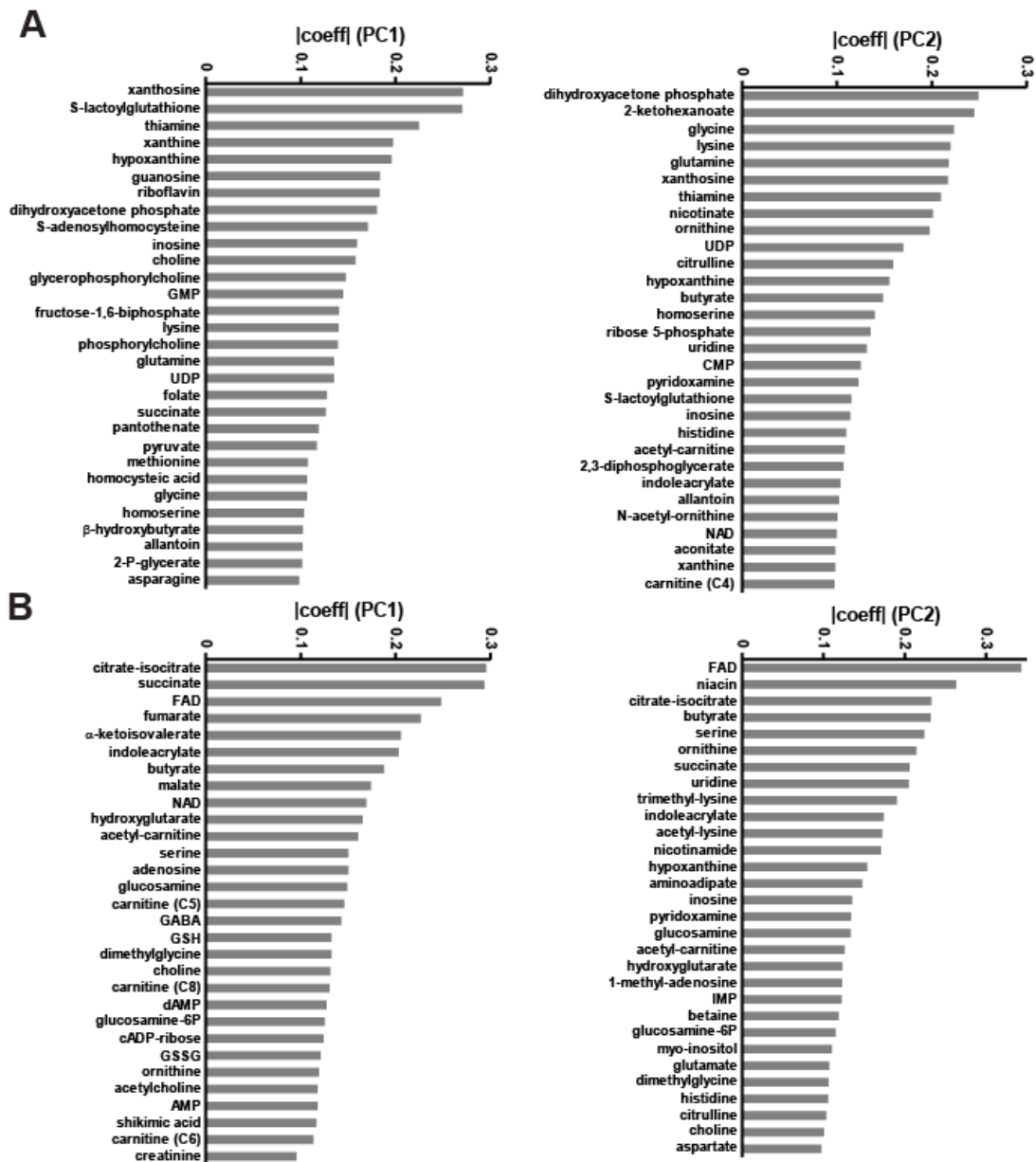
Figure S3, related to Figure 4

(A) Contribution of the top 30 metabolites contributing to principal components 1 (PC1) and 2 (PC2) for the principal component analysis of 4hr metabolomics shown in Fig. 4B. Absolute magnitude of coefficients for each metabolite for PC1 or PC2 are plotted. (B) Contribution of the top 30 metabolites contributing to PC1 and PC2 for the principal component analysis of 7 day metabolomics shown in Fig. 4D. Absolute magnitude of coefficients for each metabolite for PC1 or PC2 are plotted.

TRANSPARENT METHODS

Animal Studies

Male and female wild-type and *Nocturnin*^{-/-} C57BL/6 (congenic, N>9) mice were group-housed, under standard laboratory conditions, including a 12-hr light/dark cycle and free access to regular chow (Harlan Teklad diet 2918) and water. For cold exposure experiments, age-matched 10-20 week old young adult male and female WT and *Nocturnin*^{-/-} mice were randomly assigned to cold (6°C) or room temperature (22°C) groups. Mice were single housed for the duration (4hrs) of the experiment and food was removed in order to minimize individual variation. For the 7-day cold exposure protocol, WT and *Nocturnin*^{-/-} mice were single housed at 6°C for the duration of the experiment with free access to food and water. At the end of the experiment, mice were killed by decapitation and BAT was dissected and immediately frozen in liquid nitrogen and stored at -80°C. For the metabolomics analysis, tissue from male mice were used only. All animal studies were conducted in accordance with IACUC regulations and guidelines.

Plasmids and Cell lines

To generate the Nocturnin-FLAG lentivirus construct, the mouse Nocturnin cDNA with 3x flag tag was subcloned into the Age1 and EcorR1 sites of pLJM1-EGFP. pLJM1-EGFP plasmid was obtained from Addgene (Plasmid#19319). Single point mutants were made using Q5 Site-Directed Mutagenesis Kit according to manufacturer's instructions by some modifications. Briefly exponential amplification was performed with PCR using the primers with the point mutations mNOC (M1A), mNOC (M65A) and the template plasmid (pLJM1-mNOC). Next day, Kinase, Ligase& DpnI (KLD) treatment was performed with some modifications. Instead of using 10X KLD enzyme mix, 1μl Quick ligase, T4 PNK and Dpn1 were individually added to the mixture. Next, transformation was performed using DHSα competent cells according to manufacturer's instructions, using ampicillin selection plates. After overnight incubation at 37°C, colonies were

selected and bacterial cultures were grown with LB and the selection marker. Plasmid DNA was isolated using QIAprep Spin Miniprep Kit (Qiagen). Plasmid DNA was then sent to sequencing for the confirmation of the point mutations.

Lentiviral particles were produced according to Addgene protocol. Briefly, pLJM1-EGFP, pLJM1-NOC, pLJM1-NOC(M1A) and pLJM1-NOC(M65A) plasmids were mixed with packaging and envelope plasmids and with FUGENE Transfection Reagent (Promega) in serum-free OPTI-MEM, so that FUGENE: total DNA ratio will be 3:1. 50-80% confluent HEK-293T cells (in DMEM that does not contain antibiotics) were then transfected with this mixture. Cells were incubated at 37°C, 5% CO_2 for 12-15 hours. Next morning, transfection reagent was removed and replaced with fresh media (DMEM+10%FBS+penicillin/strepromycin). Cells were incubated for another 24 hrs at 37°C, 5% CO_2. On Days 4 and 5, lentiviral particles were collected and stored at -80°C until use.

Generating Stable Cell Lines

Immortalized mouse embryonic fibroblast (MEF) cell lines were maintained in high-glucose DMEM supplemented with 100U/ml penicillin, 10µg/ml streptomycin and 10% fetal bovine serum. To generate stable cell lines, 70% confluent MEF cells were infected with 0.1-1mL lentiviral particles. Polybrene (8µg/ml) was added to the media to increase viral infection efficacy. Titration was performed in order to assess the infection efficacy and to decide the optimal concentration of lentiviral particles for the desired gene expression level. Cells were incubated overnight and changed to fresh media after 24 hrs and selected with puromycin. Lentiviral infection was visually confirmed for the pLJM1-GFP construct and western blotting was performed to confirm the expression of other target genes.

Temperature Measurements

Wild-type and *Nocturnin*^{-/-} mice were gender-matched so that there are equal number of male and female for each genotype. Mice were single housed at 6°C with free access to food and water for the duration of the experiment and core body temperature was measured by a rectal thermometer every 4 hours (first day) and 12 hours (daily for the following 6 days). Body weight measurements were taken for mice at these same timepoints.

qRT-PCR

Total RNA was extracted from BAT tissue by Trizol (Invitrogen) using a dounce homogenizer (Wheaton). 1ug of total RNA was used to make complementary DNA using the High-Capacity cDNA Reverse Transcription kit (Applied Biosystems). Diluted cDNAs (1/100) were amplified by Power SYBR Green Master Mix (Applied Biosystems) using gene specific primers. Relative mRNA levels were calculated by quantitative PCR method and normalized to B2M gene. The following primer pairs were utilized:

Gene	Forward Primer	Reverse primer
MT-ND1(Mouse)	AATCGCCATAGCCTTCCTAA	GCGTCTGCAAATGGTTGTAA
MT-ND2 (Mouse)	CACAATATCCAGCACCAACC	GAGGCTGTTGCTTGTGTGAC
MT-CO1 (Mouse)	GGTGGTCTAACCGGAATTGT	GATAGCAAACACTGCTCCCA
MT-CO2 (Mouse)	GCCGACTAAATCAAGCAACA	CAATGGGCATAAAGCTATGG
MT-ATP8 (Mouse)	GGCACCTTCACCAAAATCACT	TGGGGTAATGAATGAGGCAAAT
MT-ATP6 (Mouse)	CAGGCTTCCGACACAAACTA	TGTAAGCCGGACTGCTAATG
MT-CO3 (Mouse)	GCCCTCCTTCTAACATCAGG	GCCTTGGTAGGTTCCTTCAC
MT-ND3 (Mouse)	AATGCGGATTCGACCCTA	TGAATTGCTCATGGTAGTGGA
MT-ND4L (Mouse)	ACTCCAACTCCATAAGCTCCA	TTTGGACGTAATCTGTTCCG
MT-ND4 (Mouse)	TATTACCCGATGAGGGAACC	AGGGCAATTAGCAGTGGAAT
MT-ND5 (Mouse)	ACCCATGACTACCATCAGCA	GGAATCGGACCAGTAGGAAA
MT-ND6 (Mouse)	AGCACAACTATATATTGCCGCTAC	GATGGTTTGGGAGATTGGTT
MT-CYTB (Mouse)	CATTCTGAGGTGCCACAGTT	GATGAAGTGGAAAGCGAAGA
MT-RNR2 (Mouse)	CCTAGGGATAACAGCGCAAT	ATCGTTGAACAAACGAACCA
MT-RNR1 (Mouse)	TGAGCAATGAAGTACGCACA	TTCCAAGCACACTTTCCAGT
mtDNA (Mouse)	CCTATCACCCTTGCCATCAT	GAGGCTGTTGCTTGTGTGAC
nDNA (Mouse)	ATGGAAAGCCTGCCATCATG	TCCTTGTTGTTCAGCATCAC
Noct-Exon3 (Mouse)	ACCAGCCAGACATACTGTGC	CTTGGGGAAAAACGTGCCT
Ucp1 (Mouse)	GGCCTCTACGACTCAGTCCA	TAAGCCGGCTGAGATCTTGT
Pparg (Mouse)	AGGCGAGGGCGATCTTGACAG	AATTCGGATGGCCACCTCTTTG
Ppargc1a (Mouse)	GAAGAGATAAAGTTGTTGGTTTGGC	AGACAAATGTGCTTCGAAAAAGAA
B2m (Mouse)	CTCGGTGACCCTGGTCTTC	TTGAGGGGTTTTCTGGATAGCA
Dio2 (Mouse)	CAGTGTGGTGCACGTCTCCAATC	TGAACCAAAGTTGACCACCAG

RNA-seq analysis

mRNA-seq libraries were prepared as previously described (Takahashi et al., 2015). Sequencing was performed by Nextseq Sequencing System (Illumina) on individually barcoded samples. Average sequencing depth was 55 million reads/sample. Using fastqc, the reads were checked for quality followed by treatment with an in-house python script to trim low quality reads. Reads were aligned with STAR (Dobin et al., 2013) against mouse genome (mm10) and gene annotation Mv14 from Gencode (Frankish et al., 2018), with parameters "--readFilesIn input.trim.gz --readFilesCommand zcat --sjdbGTFfile M14.annotation.gtf --outFilterType BySJout --outFilterMultimapNmax 10 --alignSJoverhangMin 10 --alignSJDBoverhangMin 1 --outSAMtype BAM SortedByCoordinate --outSAMunmapped Within --outFilterMismatchNmax 3 --twopassMode Basic". BAM file was filtered for ribosomal RNA and secondary alignments by keeping the uniquely mapped reads. Coverage tracks were generated using in-house python script by normalizing each sample to 10million total reads. HTSeq-count was used for raw read counting (Anders et al., 2015) and RPKM was calculated using a custom R script.

Differential gene expression analysis

The raw read counts from HTSeq-count were filtered for genes not expressed. Filtered counts were used to identify differentially expressed genes using DESeq2 (Love et al., 2014). Genes with FDR < 0.05 and $|log2(FC)| > 0.3$ were considered differentially expressed. Gene ontology analysis was performed using GOstat package in R (Falcon and Gentleman, 2007) and further confirmed with ToppGene Suite (Chen et al., 2009). Gene Ontology's categories were considered with FDR < 0.05 and number of genes per category > 5.

Co-expression network analysis

To identify modules of co-expressed genes in the RNA-seq data, we carried out weighted gene co-expression network analysis (WGCNA) (Langfelder and Horvath, 2008). A soft-threshold

power was automatically calculated to achieve approximate scale-free topology (R^2>0.85, Power = 12). Networks were constructed with blockwiseModules function with biweight midcorrelation (bicor). We used corType = bicor, maxBlockSize = 16000, mergingThresh = 0.15, reassignThreshold = 1e-6, deepSplit = 4, detectCutHeight = 0.999, minModuleSize = 30, networkType=signed. The modules were then determined using the dynamic tree-cutting algorithm. To ensure robustness of the observed network, we used a permutation approach recalculating the networks 200 times and comparing the observed connectivity per gene with the randomized one. None of the randomized networks showed similar connectivity, providing robustness to the network inference. Module visualization was performed using Cytoscape (Shannon et al., 2003). Functional enrichment was performed using GOstat package in R (Falcon and Gentleman, 2007).

Immunocytochemistry and Confocal Microscopy

Standard immunocytochemistry protocols were used. Briefly, cells were washed twice with PBS, incubated with 300nM MitoTracker Red CMXRos for 30 minutes at 37°C prior to fixation (4%PFA, 37°C, 10 minutes). Cells were then washed 3 times with PBS, permeabilized (0.2% TritonX/PBS, 10 minutes), blocked (3%BSA/PBS for 30 minutes) and incubated overnight with the primary antibody (αFLAG M2 (Sigma F1804)) added to the blocking solution. The next day, cells were washed 3 times with PBS and incubated with secondary antibody (AlexaFluor 488 (Life Technologies)), followed by DAPI (5 min). After another wash cells were mounted onto coverslips. Confocal images were acquired using a Zeiss LSM710 confocal microscope, and images were analyzed using Zen software.

Mitochondrial Respiration Assay

Cellular respiration was measured using the Seahorse XFe96 analyzer (Seahorse Biosciences, Agilent technologies). Briefly, 14,000 cells were plated into micro well plates the night before the assay. The next day, the cell culture media was replaced with assay media (DMEM (Sigma D5030) supplemented with 10% FBS, 1% penicillin/streptomycin, 2mM glutamine, 1mM pyruvate, 10mM glucose). Cells were equilibrated to the assay media for one hour (37°C) before analysis. The final concentrations for drugs used in the experiment were: oligomycin (2μM), CCCP (10μM) and antimycinA (2μM). Protein concentrations were calculated using a BCA assay kit (ThermoFisher), and used to normalize oxygen consumption measurements.

Mitochondrial respiration in permeabilized cells (10,000 cells / well) was measured using the XF PMP reagent (Agilent Technologies), according to manufacturer's instructions. Briefly, cells were exchanged into assay buffer (2mM HEPES, 220mm mannitol, 70mM sucrose, 10mM KH_2PO_4, 5mM $MgCl_2$, 1mM EGTA, pH7.4), supplemented with 2nM PMP reagent, and either complex I substrates (10mM pyruvate, 1mM malate) or complex II substrate (10mM succinate, 2μM rotenone). Oxygen consumption was measured under basal conditions and following injection of antimycin A (final concentration 2uM) in order to calculate state 4 (uncoupled) mitochondrial respiration.

DNA Extraction

Mitochondrial and genomic DNA was extracted from BAT tissue using DNeasy Blood and Tissue Kit (QIAGEN) according to manufacturer's instructions. 10ng of DNA was then amplified by qRT-PCR using primers for genomic and mitochondrial DNA.

Mitochondrial Fractionation and Proteinase K Assay

Mitochondrial isolation was performed as previously described (Frezza et al., 2007). Briefly, five confluent 10cm plates of HEK 293 cells were collected using a cell scraper, then resuspended in

3ml of isolation buffer (10mM HEPES, 220mM mannitol, 70mM sucrose, 5mM $MgCl_2$, 1mM EGTA, 20mM KCl, pH7.4). Approximately 1,000,000 cells were collected, spun down, and lysed in 100ul of RIPA buffer for the whole-cell lysate. The rest of the cell suspension was mechanically disrupted using a glass-Teflon dounce homogenizer. The lysates were spun down at 600g for 10 minutes at 4°C to pellet unbroken cells and nuclei. The supernatant was collected and centrifuged again at 7,000g for 10 minutes at 4°C to pellet the mitochondrial fraction. The mitochondrial pellet was washed with 200ul of isolation buffer and then equally split into 7 different microcentrifuge tubes. The pellet was spun down at 7,000g for 10 minutes at 4°C, and the supernatant was discarded. The mitochondrial pellets were resuspended in 40ul of reaction buffer. Briefly, 100μg/ml Proteinase K and/or 1%TritonX-100 were added to the samples in isolation buffer and samples were incubated on ice for 30 minutes. The reaction was stopped by the addition of 2ul of 100mM PMSF and 10ul of 5x SDS sample buffer. Ten microliters of each sample were loaded for SDS-PAGE and Western blot analysis, probing with antibodies raised against: Tubulin (Sigma T6199), Nocturnin (in house antibody ((Niu et al., 2011)), and MT-CO1 (Invitrogen 459600). Mitochondrial fractionation from BAT was similarly performed, and extracts were probed with antibodies against Nocturnin (in house antibody (Niu et al., 2011)), VDAC (Cell Signaling D73D12), MT-CO2 (Proteintech 55070-1-AP), and Actin (Millipore MAB1501).

BAT Metabolomics

Frozen BAT tissue (50-100mg) was homogenized in chloroform/methanol/H_2O (40:40:20), and metabolites were extracted from the polar layer. Samples were subjected to three freeze-thaw cycles, and spun at 14000rpm for 15min to pellet precipitants. The supernatant was transferred to a new tube and evaporated overnight. For LC-MS/MS measurements, dried metabolites were resuspended in 0.03% formic acid, vortexed and centrifuged to remove debris. Samples were randomized and blinded prior to analysis on an AB QTRAP 5500 liquid chromatograph/triple quadropole mass spectrometer (Applied Biosystem SCIEX). Chromatogram review and peak

area integration was performed in MultiQuant software. Peak areas were normalized against total ion count.

Statistical Analysis

Statistical analysis was performed using GraphPad Prism software. Two-way analysis of variance (ANOVA) followed by *post hoc* tests or two-tailed Student's t-tests were performed as indicated. For metabolomics, hierarchical clustering was performed in Cluster 3.0, and principal component analysis was performed in MATLAB (MathWorks, Inc.).

Availability of data and material

The NCBI Gene Expression Omnibus (GEO) accession number for the data reported in this manuscript is **GSE133050 (token: yvmregeultsvtih).**

References

Anders, S., Pyl, P.T., and Huber, W. (2015). HTSeq--a Python framework to work with high-throughput sequencing data. Bioinformatics *31*, 166-169.

Chen, J., Bardes, E.E., Aronow, B.J., and Jegga, A.G. (2009). ToppGene Suite for gene list enrichment analysis and candidate gene prioritization. Nucleic Acids Res *37*, W305-311.

Dobin, A., Davis, C.A., Schlesinger, F., Drenkow, J., Zaleski, C., Jha, S., Batut, P., Chaisson, M., and Gingeras, T.R. (2013). STAR: ultrafast universal RNA-seq aligner. Bioinformatics *29*, 15-21.

Falcon, S., and Gentleman, R. (2007). Using GOstats to test gene lists for GO term association. Bioinformatics *23*, 257-258.

Frankish, A., Diekhans, M., Ferreira, A.M., Johnson, R., Jungreis, I., Loveland, J., Mudge, J.M., Sisu, C., Wright, J., Armstrong, J., et al. (2018). GENCODE reference annotation for the human and mouse genomes. Nucleic Acids Res.

Frezza, C., Cipolat, S., and Scorrano, L. (2007). Organelle isolation: functional mitochondria from mouse liver, muscle and cultured fibroblasts. Nat Protoc *2*, 287-295.

Langfelder, P., and Horvath, S. (2008). WGCNA: an R package for weighted correlation network analysis. BMC Bioinformatics *9*, 559.

Love, M.I., Huber, W., and Anders, S. (2014). Moderated estimation of fold change and dispersion for RNA-seq data with DESeq2. Genome Biol *15*, 550.

Michel, A.M., Fox, G., A, M.K., De Bo, C., O'Connor, P.B., Heaphy, S.M., Mullan, J.P., Donohue, C.A., Higgins, D.G., and Baranov, P.V. (2014). GWIPS-viz: development of a ribo-seq genome browser. Nucleic Acids Res *42*, D859-864.

Niu, S., Shingle, D.L., Garbarino-Pico, E., Kojima, S., Gilbert, M., and Green, C.B. (2011). The circadian deadenylase Nocturnin is necessary for stabilization of the iNOS mRNA in mice. PloS one *6*, e26954.

Shannon, P., Markiel, A., Ozier, O., Baliga, N.S., Wang, J.T., Ramage, D., Amin, N., Schwikowski, B., and Ideker, T. (2003). Cytoscape: a software environment for integrated models of biomolecular interaction networks. Genome Res *13*, 2498-2504.

Smith, A.C., and Robinson, A.J. (2016). MitoMiner v3.1, an update on the mitochondrial proteomics database. Nucleic Acids Res *44*, D1258-1261.

Takahashi, J.S., Kumar, V., Nakashe, P., Koike, N., Huang, H.C., Green, C.B., and Kim, T.K. (2015). ChIP-seq and RNA-seq methods to study circadian control of transcription in mammals. Methods Enzymol *551*, 285-321.